Time reversal of ocean noise

Philippe Roux[a] and W. A. Kuperman
Marine Physical Laboratory, Scripps Institution of Oceanography, University of California, San Diego, La Jolla, California 92093-0238

(Received 9 July 2004; revised 5 September 2004; accepted 29 September 2004)

It has recently been shown [Roux *et al.*, ''Extracting coherent wave fronts from acoustic ambient noise in the ocean,'' J. Acoust. Soc. Am. **116**, 1995–2003 (2004)] that the time-averaged correlation of ocean noise between two points yields a deterministic waveguide arrival structure embedded in the time-domain Green's function. By performing a set of these correlations between a vertical receive array and a single receiver, transfer functions necessary for time reversal can be extracted from ocean noise. Theory and simulation demonstrate this process and data of opportunity from the North Pacific Acoustic Laboratory experiment confirm the expected performance of a noise-based time reversal mirror. © *2005 Acoustical Society of America.* [DOI: 10.1121/1.1834616]

PACS numbers: 43.30.Pc, 43.50.Rq, 43.60.Tj [WLS] Pages: 131–136

I. INTRODUCTION

The experimental implementation of an acoustic time reversal mirror (TRM) is now well established both in underwater acoustics[1–3] and in ultrasonics.[4–6] Time reversal is based on reciprocity and time symmetry of the wave equation and the *coherent* recombination of acoustic fields. The extension of the TRM process to *a priori* incoherent noise fields is, therefore, not immediately intuitive. However, since it has recently been shown[7] that the time-averaged correlation function of ocean noise between two points yields deterministic wave fronts related to the structure of the time domain Green's function (TDGF) between those two points, a noisebased TRM would, nevertheless, appear a possibility. Indeed, theory and simulation demonstrate this process[8] and data of opportunity from the North Pacific Acoustic Laboratory experiment[9] confirm the expected performance of a noise-based TRM (NTRM).

The basic configuration of a TRM experiment in the ocean is shown in Fig. 1(a). A probe source S emits a pulse that is received on an array [Fig. 1(b)], time-reversed, and re-emitted. After time reversal, the resulting field focuses back at the probe source position [Fig. 1(c)]. For a noise-based TRM, the noise-extracted TDGF between a surrogate probe source S′ and one element of the array [Fig. 1(d)] is obtained passively via a noise correlation process[10] as indicated in Fig. 1(e). Indeed, the time-averaged cross correlation of ambient noise yields a two-sided symmetric signal that corresponds to an incoming and outgoing wave between S′ and the array [Fig. 1(e)]. As explained in Sec. III of this paper, the outgoing wave is composed of amplitude-shaded noise-extracted TDGFs, the shading being the signature of predominant surface noise sources in the ambient noise field [Fig. 1(d)]. As with a regular TRM, a NTRM experiment then consists of reemitting the noise-extracted TDGFs from the array [Fig. 1(f)]. At this point, there are two options for carrying out the second step of the time-reversal process:

(1) Active time reversal: implement the time reversal process by actually transmitting the time-reversed noise-extracted TDGFs from the array.
(2) Passive time reversal: implement the time reversal process numerically by correlating the noise-based TDGFs obtained from different time-domain ambient noise realizations.

We show in this paper from numerical and experimental data that both active and passive NTRM focus the time-reversed noise correlation function back to the surrogate probe source S′. The potential value of passive NTRM is that it suggests a totally passive (source less) matched field tomography based on the degradation associated with a time changing environment. On the other hand, as shown in Sec. III, because the noise-extracted TDGFs are different from the actual TDGFs, the focus that results from passive NTRM, active NTRM, and classical TRM may differ.

The main advantage of NTRM over TRM relies in the passive way the noise-extracted TDGFs are acquired with a NTRM, for which no probe source is required. However, a NTRM needs a connection between S′ and the array, which may not be practical with distant arrays. Another drawback of NTRM is the necessary time average to observe the convergence of the ambient noise correlation process to the noise-extracted TDGFs. Actually, a NTRM experiment will only be possible when the time scale of the medium fluctuations will be longer than the convergence time of the noise correlation process.[8] This issue is addressed with experimental data in Sec. IV. The paper is structured as follows: In Sec. II, we present the theory of the noise-based TRM. Section III shows results from numerical simulations while Sec. IV confirms the formulation with experimental data.

II. THEORY OF A NOISE-BASED TRM

In the following we show that we obtain a TRM from the noise correlation process. First we write down the classical TRM result; next we review the structure of the output

[a]Electronic mail: proux@ucsd.edu

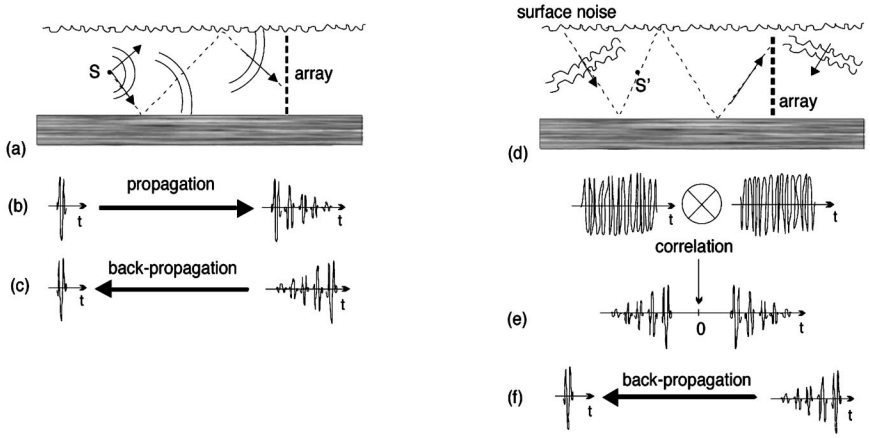

FIG. 1. (a) Classical configuration for a time-reversal mirror (TRM). (b) A probe source S transmits a signal to a source receive array where it is time reversed and retransmitted at each element of the array. (c) The backpropagated field focuses at the source position. (d) Configuration for a noise-based time reversal mirror (NTRM). A noise-extracted TDGF is obtained by retaining the positive time side of the noise correlation function (e) between a surrogate probe source S′ and each element of the array (Ref. 9). Though different in amplitude, this signal is phase-matched to the signal obtained on the array from the probe source in (b). The subsequent backpropagation (f) is the same as in the classical TRM. A variation is to computationally perform (f) but with an independent set of noise-extracted TDGFs taken at another time interval. The degree to which the ocean is temporally stable will be reflected in the quality of the focus.

of the temporal noise correlation. Finally we insert this result into the classically derived TRM result to obtain the noise-based TRM process.

A. Classical TRM

For the geometry shown in Fig. 1, the phase conjugated (frequency analog of time reversal) pressure field P_{pc} from a vertical line of J discrete sources, is classically defined as[11,12]

$$P_{\mathrm{pc}}(r,z,\omega)=\sum_{j=1}^{\mathrm{J}} G_{\omega}(r,z;R,z_j)G_{\omega}^{*}(R,z_j;0,z_{\mathrm{ps}}), \tag{1}$$

where $G_{\omega}^{*}(R,z_j;0,z_{\mathrm{ps}})$ represents the complex-conjugated frequency-dependent Green's function from the probe source at depth z_{ps} to each element of the array at range R and depth z_j. Similarly $G_{\omega}(r,z;R,z_j)$ is the Green's function from each array element back to range r and depth z around the probe source position.

We obtain the time domain version of Eq. (1) by first Fourier synthesizing a pulse at the jth array element,

$$P(R,z_j,t)=\int G_{\omega}(R,z_j;0,z_{\mathrm{ps}})S(\omega)e^{-i\omega t}d\omega, \tag{2}$$

where $S(\omega)$ is the Fourier transform of the probe source pulse. For constant $S(\omega)$, Eq. (2) is proportional to the time domain Green's function, $G_t(R,z_j;0,z_{\mathrm{ps}})$. This expression incorporates all waveguide effects, including time elongation due to multipath propagation. For convenience, we take the time origin such that $P(R,z_j,t)=0$ outside the time interval $(0,\tau)$. The time-reversed signal that will be used to excite the jth transmitting array element is $P(R,z_j,T-t)$ such that $T>\tau$. This condition is imposed by causality. The signal has to be completely received before it can be time reversed. Then, we have

$$\begin{aligned}P(R,z_j,T-t)&=\int G_{\omega}(R,z_j;0,z_{\mathrm{ps}})S(\omega)e^{-i\omega(T-t)}d\omega\\&=\int [\mathrm{G}_{\omega}^{*}(R,z_j;0,z_{\mathrm{ps}})e^{i\omega T}S^{*}(\omega)]e^{-i\omega t}d\omega,\end{aligned} \tag{3}$$

where the sign of the integration variable, ω, has been reversed and the conjugate symmetry of the frequency-domain Green's function and the probe source signal have been used. The quantity in square brackets in Eq. (3) is the Fourier transform of the signal received by the jth array element after time reversal. The time delay confirms the equivalence of time reversal and phase conjugation in their respective time and frequency domains.

Noting that the bracketed quantity in Eq. (3) contains the frequency domain representation of the signal retransmitted by the jth array element, Fourier synthesis can be used to obtain the time-domain representation of the field produced by the TRM. From Eq. (1), we have

$$\begin{aligned}P_{\mathrm{TRM}}(r,z,t)=\sum_{j=1}^{J}\int G_{\omega}(r,z;0,z_j)G_{\omega}^{*}(R,z_j;0,z_{\mathrm{ps}})\\\times e^{i\omega T}S^{*}(\omega)e^{-i\omega t}d\omega.\end{aligned} \tag{4}$$

This expression can be used to show that the TRM produces focusing in time as well as in space. Focusing in time occurs because a matched filter occurs. To understand this, examine the TRM field at the focal point [that is, take $r=0$, $z=z_{\mathrm{ps}}$ in Eq. (4)]. The time-domain equivalent of Eq. (4) is

$$\begin{aligned}P_{\mathrm{TRM}}(0,z_{\mathrm{ps}},t)=\frac{1}{(2\pi)^2}\sum_{j=1}^{J}\int\int G_{t''+t'}(0,z_{\mathrm{ps}};R,z_j)\\\times G_{t'}(R,z_j;0,z_{\mathrm{ps}})S(t''+T-t)dt'dt'',\end{aligned} \tag{5}$$

where $G_{t'}(R,z_j;0,z_{\mathrm{ps}})$ represents the TDGF at time t' from the probe source at depth z_{ps} to each array element at range R and depth z_j. Similarly $G_{t''+t'}(0,z_{\mathrm{ps}};R,z_j)$ is the TDGF at

time $t''+t'$ from each array element back to the source at depth z_{ps}. If reciprocity holds in the medium, the TDGF satisfies the condition:

$$G_{t''+t'}(0,z_{ps};R,z_j)=G_{t''+t'}(R,z_j;0,z_{ps}). \quad (6)$$

Using Eq. (6), we observe that the integration over t' in Eq. (5) is an autocorrelation of the Green's function. This operation is matched filtering, with the filter matched to the impulse response from the probe source to the jth array element. The summation is then performed on the J elements of the TRM. Finally, note that the integral over t'' in Eq. (5) is a convolution of each matched-filtered channel impulse response with the time reversed and delayed probe pulse. The signal $S(t''+T-t)$ is the time reversed version of the original probe source signal and the derivation of Eq. (5) uses the causality requirement, $T>\tau$.

B. The TDGF from noise correlation

We omit repeating the well-known normal mode waveguide theory.[13] The frequency domain correlation function of ocean surface generated noise between the probe source and one element of the array is approximated by[10]

$$C_\omega(R,z_{ps},z_j)=\frac{\pi q(\omega)^2}{2\rho^2 k^2}\sum_m \frac{[u_m(z')]^2}{\alpha_m\kappa_m} \times u_m(z_{ps})u_m(z_j)J_0(\kappa_m R). \quad (7)$$

The derivation of Eq. (7) assumes that the modal attenuation coefficients α_m are much smaller than the smallest separation between the real part κ_m of the wave numbers (which is common in underwater acoustics); $u_m(z)$ are the depth dependent mode shape; $q(\omega)$ is the strength of the noise sources, and z' is the depth of the noise layer. Since the Bessel Function $J_0(\kappa_m R)$ is the sum of two Hankel functions of opposite sign, $J_0(\kappa_m R)=\frac{1}{2}(H_0^{(1)}(\kappa_m R)+H_0^{(1)}(-\kappa_m R))$, Eq. (7) can be rewritten as in[9,12]

$$C_\omega(R,z_{ps},z_j)=\frac{\pi q(\omega)^2}{4\rho^2 k^2}\sum_m \frac{[u_m(z')]^2}{\alpha_m\kappa_m}u_m(z_{ps})u_m(z_j) \times[H_0^{(1)}(\kappa_m R)+H_0^{(1)}(-\kappa_m R)] \equiv C_\omega^{(\mathrm{in})}(R,z_{ps},z_j)+C_\omega^{(\mathrm{out})}(R,z_{ps},z_j). \quad (8)$$

Aside from the amplitude shading represented by the fraction in the modal sum of Eq. (8), the frequency domain noise correlation function is composed of the ingoing $C_\omega^{(\mathrm{in})}$ and outgoing $C_\omega^{(\mathrm{out})}$ waveguide Green's function. The shading term $[u_m(z')]^2/\alpha_m\kappa_m$ indicates that the modes amplitude results from near surface, dipole-like excitation of sources distributed over an infinite surface. Since this shading term is real, the structure of the resulting time domain correlation function will have the same temporal structure as the TDGF, but with wave front amplitude determined by the shading. We illustrate this in Fig. 2 where the TDGF in the waveguide is plotted together with the outgoing part of the time domain noise correlation function as computed from the Fourier transform of the frequency domain noise correlation function. Both signals have been weighted by a Gaussian-shaped spectrum between 70 and 130 Hz. The noise correlation function has been computed from a full-field integration code[10,14] in order to further confirm the precise relationship with the TDGF. As expected from Eq. (8), Figs. 2(a) and (b) exhibit the same wave front structure with different amplitude modulation. Figure 2(c) further confirms that the TDGF and the noise correlation function can be superimposed aside from the relative amplitudes of their modal components. Because time reversal is known to be more sensitive to phase than amplitude mismatch,[6] the noise correlation function may be used as a powerful approximation of the TDGF to perform time reversal. Finally, note that the dependence of the noise correlation function versus the noise layer depth z' is studied in detail in Ref. 8.

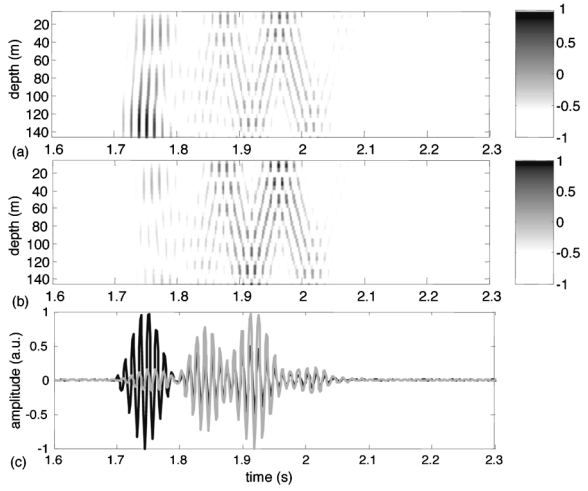

FIG. 2. Spatial-temporal representation of the acoustic field in a 150-m-deep shallow water waveguide. (a) The classical TDGF is computed between 70 and 130 Hz for a 125-m-deep point source as received on a vertical array at range 2500 m. (b) The noise-extracted TDGF for the same geometry and frequency bandwidth showing greater amplitudes of higher modes (i.e., later arrivals) due to the dipole shading of the original noise sources (Ref. 9). The contrast of the gray colorbar has been enhanced to better demonstrate that the temporal structures of both panels are the same. (c) Classical TDGF (black line) and noise-extracted TDGF (gray line) obtained at the source depth. The sound speed profile in the waveguide decreases linearly from 1500 m/s at the surface to 1470 m/s at the bottom. The bottom sound speed, density, and attenuation are 1800 m/s, 1800 kg/m^3, and 0.1 dB/λ, respectively.

C. Noise-based TR

Since there are no factors that would alter the mathematics used in going to the time domain representation of the noise correlation function, we can immediately consider the Fourier transform of Eq. (8) to be the two sided version of the noise-extracted TDGF. Consequently, after selecting the outgoing wave of the time domain noise correlation function, the passive noise-based time reversal analog of Eq. (5) is

$$P_{\mathrm{NTRM}}^{\mathrm{passive}}(0,z_{ps},t)=\frac{1}{(2\pi)^2}\sum_{j=1}^{J}\int\int C_{t''+t'}^{(\mathrm{out})}(R,z_{ps},z_j)C_{t'}^{(\mathrm{out})} \times(R,z_j,z_{ps})S(t''+T-t)dt'dt'', \quad (9)$$

with

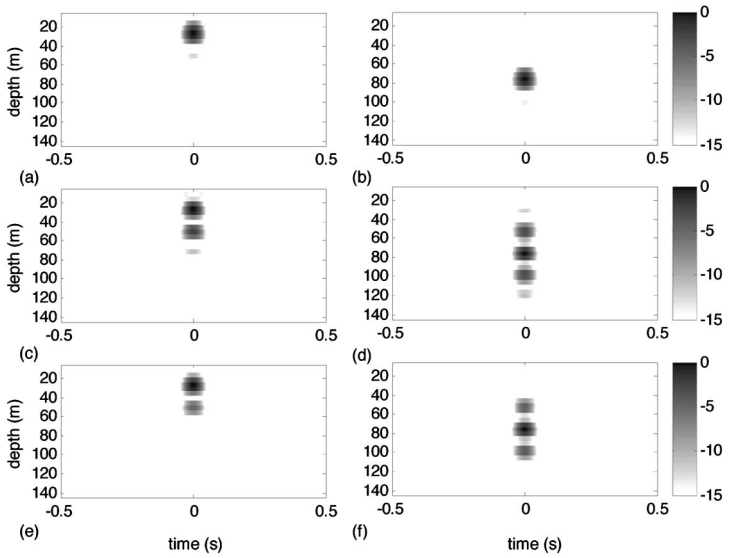

FIG. 3. Spatial-temporal representation of time reversal focal spots computed between 70 and 130 Hz for two different probe source or surrogate probe source positions at depth 25 and 75 m, respectively. (a), (b) Classical TRM; (c), (d) passive NTRM; (e), (f) active NTRM. The latter simulates an actual retransmission for the second step of the TRM process. In each case, time reversal is performed from a 29-element array that covers the whole water column. The waveguide characteristics are the same as in Fig. 2.

$$C_t^{(\mathrm{out})}(R,z_{\mathrm{ps}},z_j)=\int C_\omega^{(\mathrm{out})}(R,z_{\mathrm{ps}},z_j)S(\omega)e^{-i\omega t}d\omega. \tag{10}$$

We retain the source spectrum term in Eq. (4) as a reminder that the noise correlation will cover a finite bandwidth; typically we take the noise spectrum to be constant over this bandwidth. Equation (9) represents the passive NTRM process in which the noise data are used for both the forward and backward components of the TRM process. For active NTRM, in which the time reversal is actually performed by retransmission at the array, we have

$$P_{\mathrm{NTRM}}^{\mathrm{active}}(0,z_{\mathrm{ps}},t)=\frac{1}{(2\pi)^2}\sum_{j=1}^{j}\int\int G_{t''+t'}(0,z_{\mathrm{ps}};R,z_j)\times C_{t'}^{(\mathrm{out})}(R,z_j,z_{\mathrm{ps}})S(t''+T-t)dt'dt''. \tag{11}$$

Comparing Eqs. (5), (9), and (11), we see that TRM is not equivalent to passive/active NTRM because the noise correlation function (which outgoing part is defined as the noise-extracted TDGF) differs from the actual TDGF.

III. SIMULATION OF A NOISE BASED TRM

Figure 3 shows the results of NTRM simulation where we use the correlation of noise between a receiver that acts as a surrogate probe source and an array of receivers that performs the role of a TRM. We show the spatial temporal time reversal focal spots corresponding to both Eqs. (10) (passive NTRM) and (11) (active NTRM) as well as to Eq. (5), i.e., the classical TRM procedure. The simulation is full field[14] so as not to exclude the continuous spectrum part of the waveguide Green's function. The focusing examples are for a surrogate probe source at two different depths and the three cases discussed above: classical TRM, passive and active NTRM.

The main difference between the NTRM focal spots and the classical TRM is the sidelobe structure as shown in greater detail in Fig. 4. The classical TRM has minimum sidelobes and the next best performance is active NTRM. The difference between classical and the passive noise-based TRM arises from the fact that the surface noise modal distribution is weighted toward higher modes (see Fig. 2 or Ref. 7) and therefore cannot be used to fully reconstruct a point source in the diffraction limit. The reason that the active NTRM has better sidelobe performance than the passive NTRM is that the former is closely related to the classical TRM with higher modes being shaded only in the second step of the TRM process rather than having the full, effective two-way shading of the latter.

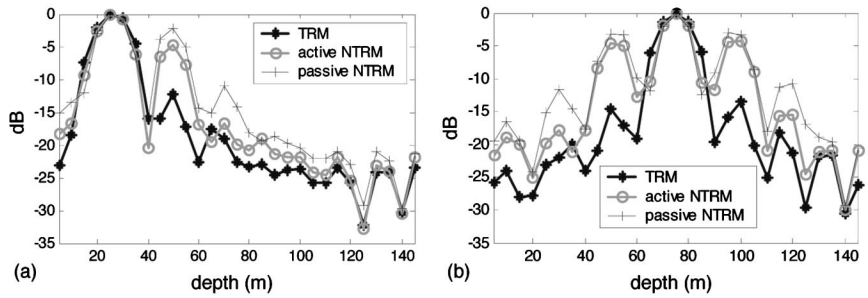

FIG. 4. The depth-dependent focal spot structure for the examples in Fig. 3. (a) and (b) correspond to probe source or surrogate probe source at depth 25 and 75 m, respectively. Classical TRM exhibits lower sidelobes. Active NTRM retransmission has the second best focal spot structure; in this case, the amplitude shading of the noise-extracted TDGFs only impacts the forward propagation. For the passive NTRM, this shading is present in both forward and backward propagations, leading to higher sidelobes.

IV. EXPERIMENTAL DEMONSTRATION OF A NOISE-BASED TRM

The experimental requirement for a NTRM is the ability to perform correlations of noise at distant hydrophones; hence there is a requirement for highly accurate time synchronization between receivers. The North Pacific Acoustic Laboratory experiments[7,9] provide such data to demonstrate the feasibility of implementing a noise-based TRM. We have already shown[7] that even though the NPAL data were basically shipping and not surface-generated noise, the long time correlation process leads to comparable results for both types of data.

Figure 5 is a schematic of the NPAL experiment in the context of a NTRM. With data, we work directly in the time domain so that the inverse Fourier transform of Eq. (8) is simply

$$C_t(R,z_{\mathrm{ps}},z_j)=\int_0^{T_N} N(R,z_j,t')N(0,z_{\mathrm{ps}},t+t')dt'$$

$$\equiv C_t^{(\mathrm{in})}(R,z_{\mathrm{ps}},z_j)+C_t^{(\mathrm{out})}(R,z_{\mathrm{ps}},z_j), \qquad (12)$$

where $N(0,z_{\mathrm{ps}},\mathrm{t})$ and $N(R,z_j,t)$ are the ambient noise received simultaneously at time t on two receivers on different arrays. T_N is the time interval on which ambient noise has been recorded. In the case of the NPAL data, we used time segments $T_N=5$ min. In the case of shipping noise, this time interval appears to be long enough in the studied frequency bandwidth [70–130 Hz] to allow the convergence of the noise correlation function to the noise-extracted TDGF as written in the lower part of Eq. (12). From the two-sided noise correlation function, we retain only the positive time side, $C_t^{(\mathrm{out})}(R,z_{\mathrm{ps}},z_j)$ for the NTRM implementation.

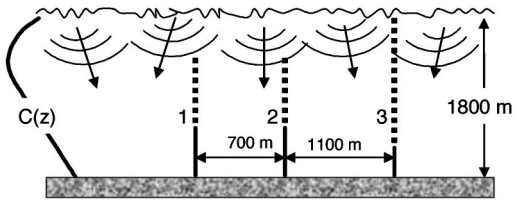

FIG. 5. Schematic of the NPAL experimental setup used for constructing the NTRM process. Array 3 (composed of 40 hydrophones with a 35 m array pitch) is twice as long as arrays 1 and 2 (20 hydrophones with a 35 m array pitch). All the arrays are synchronized permitting accurate cross-correlation. The time-domain noise correlation function between arrays 3 and 2 and arrays 1 and 2 will be used to construct the noise-extracted TDGFs on arrays 1 and 3 with the surrogate probe sources being located on array 2.

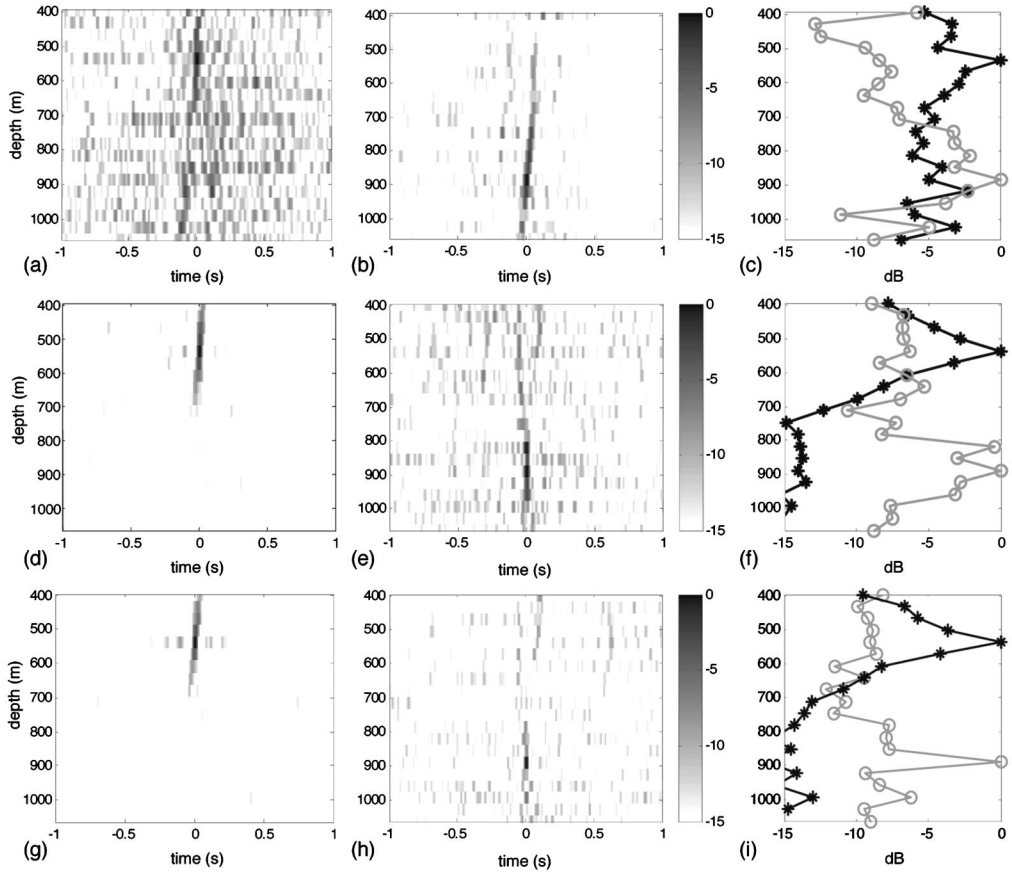

FIG. 6. Spatial temporal representation of the focal spots obtained with passive NTRM from ambient noise data recorded during the NPAL experiment as configured in Fig. 5. We use two different 5 min time intervals for the noise correlation function providing the forward and backward propagating noise-extracted TDGFs. The surrogate probe sources on array 2 are located at depths 536 and 887 m. (a) and (b) Passive NTRM performed from array 1 onto array 2 at the two depths, respectively. (d) and (e) Passive NTRM performed from array 3 onto array 2 at the two depths, respectively. Note that the focus is better because array 3 is larger than array 1. (g) and (h) Passive NTRM performed simultaneously from arrays 1 and 3 onto array 2 at the two depths, respectively. The combined focus at the deeper depth (h) displays a much sharper focus than the single array passive NTRM results of (b) and (e); this is strong evidence that we have constructed a *coherent* NTRM process. (c), (f), (i) The right-hand panels show the depth-dependent focal spot structures at array 2 at depth 536 m (in black), and at depth 887 m (in gray).

Figure 6 shows the spatial temporal focal spot in the case of the passive NTRM. In order to avoid circular reasoning in constructing this result, passive NTRM is performed in two steps. First, $T_N = 5$ min of data are used to obtain the noise-extracted TDGFs by correlating ambient noise between one receiver on array 2 and the other two arrays. In a second step, a different interval $T_N = 5$ min is used to construct the noise-extracted TDGFs that will be used to virtually backpropagate the time-reversed field to the receiver on array 2. The time-reversal results are consistent with what we expect from the classical TRM process. For the larger array refocusing onto array 2 [Figs. 6(d)–(f)] we have a better focus than from the smaller one [Figs. 6(a)–(c)]. Further, the combination of both arrays refocusing at array 2 gives the best focus [Figs. 6(g)–(i)]. For the latter case, the sharper focus observed on the deeper array element can only be explained by a constructive interference between the time reversed fields issued from arrays 1 and 3. This confirms that a TRM-like coherent process occurred from arrays 1 and 3 back to array 2.

V. DISCUSSION

The successful oceanic implementation of NTRM relies on the efficiency of the ambient noise cross-correlation process to extract coherent wave fronts between a surrogate probe source and a hydrophone array. As detailed in Ref. 8, the noise correlation process yields a good estimation of the TDGF when a series of requirements are fulfilled. First, the use of time-synchronized receivers and the absence of strong motions between them (relative to the wavelength) are required. The dynamic range of the hydrophones should be such that low ambient noise can be distinguished from electronic noise. This means also an adequate balance between the medium attenuation and the range separating the pseudosource and the array. As such, the NPAL data provided an excellent example of multiarray noise measurements satisfying these conditions. Second, the choice of the recording time is driven by the need to record a sufficient number of uncorrelated noise events. Thus, hydrophones with large frequency bandwidth work in favor of the noise-correlation process. Naturally, the recording time should also be smaller than the fluctuations time-scale of the environment. Third, the noise correlation process will converge faster toward the noise-extracted TDGF when a homogeneous distribution, in space and time, of uncorrelated noise sources are present. When this condition is not satisfied (ship passing by, burst of sound from marine mammals), temporal or frequency equalization will be necessary to remove high energy single events.

In conclusion, we have shown in this paper by theory and simulation that a noise-based time-reversal mirror is feasible. We have also used data of opportunity to confirm our results. The data confirm that ambient noise from two separate time intervals can be used to construct the required transfer functions for the propagation and backpropagation stages of the time-reversal process. The reason we use the word ''confirm'' and not ''prove'' with respect to the data is that there is a time-averaged correlation requirement. This time interval is dependent on specific environmental and shipping conditions[7] that we do not know for certain in the case of the data presented in this paper. Actually, the convergence of the noise correlation process in general is still very much a research issue.[8,15] However, the multiarray demonstration of a passive NTRM as explained earlier is further compelling evidence of the basic process. Theory and simulation prove the feasibility of NTRM within their respective domains. What still remains to be experimentally demonstrated is active NTRM, in which the noise data on a TRM representing a surrogate probe source can be re-emitted by a set of sources and refocused at the surrogate probe source.

ACKNOWLEDGMENT

This research was supported by the Office of Naval Research.

[1] A. Parvulescu and C. S. Clay, ''Reproducibility of signal transmissions in the ocean,'' Radio Electron. Eng. **29**, 223–228 (1965).
[2] W. A. Kuperman, W. S. Hodgkiss, H. C. Song, T. Akal, C. Ferla, and Darell Jackson, ''Phase Conjugation in the ocean: Experimental demonstration of an acoustic time-reversal mirror,'' J. Acoust. Soc. Am. **103**, 25–40 (1998).
[3] S. Kim, G. G. Edelmann, W. A. Kuperman, W. S. Hodgkiss, H. C. Song, and T. Akal, ''Spatial resolution of time-reversal arrays in shallow water,'' J. Acoust. Soc. Am. **110**, 820–829 (2001).
[4] M. Fink, C. Prada, F. Wu, and D. Cassereau, ''Self focusing with time reversal mirror in inhomogeneous media,'' Proceedings of IEEE Ultrasonics Symposium, 2, Montreal, 1989, pp. 681–686.
[5] M. Fink, ''Time reversed acoustics,'' Phys. Today **50**, 34–40 (1997).
[6] P. Roux and M. Fink, ''Time-reversal in a waveguide: Study of the spatial and temporal focusing,'' J. Acoust. Soc. Am. **107**, 2418–2429 (2000).
[7] P. Roux, W. A. Kuperman, and the NPAL Group, ''Extracting coherent wave fronts fom acoustic ambient noise in the ocean,'' J. Acoust. Soc. Am. **116**, 1995–2003 (2004).
[8] K. G. Sabra, P. Roux, and W. A. Kuperman, ''Time delays structure of the long-time ambient noise cross-correlation function in an oceanic waveguide,'' J. Acoust. Soc. Am. (in press).
[9] The ATOC Consortium (A. B. Baggeroer, T. G. Birdsall, C. Clark, J. A. Colosi, B. D. Cornuelle, D. Costa, B. D. Dushaw, M. Dzieciuch, M. G. Forbes, C. Hill, B. M. Howe, J. Marshall, D. Menemenlis, J. A. Mercer, K. Metzger, W. Munk, R. C. Spindel, D. Stammer, P. F. Worcester, and C. Wunsch), Science **281**, 1327–1332 (1998). The North Pacific Acoustic Laboratory (NPAL) experiments were designed to study coherence of acoustic signal propagating long distances in the ocean. The acoustic source was 3000 km from the arrays. The NPAL group (J. A. Colosi, B. D. Cornuelle, B. D. Dushaw, M. A. Dzieciuch, B. M. Howe, J. A. Mercer, W. Munk, R. C. Spindel, and P. F. Worcester) provided us with noise data from their receiver array during times when their source was not transmitting. Their array technology is the same used in the Acoustic Thermometry of the Ocean Climate experiments.
[10] W. A. Kuperman and F. Ingenito, ''Spatial correlation of surface generated noise in a stratified ocean,'' J. Acoust. Soc. Am. **67**, 1988–1996 (1980).
[11] D. R. Jackson and D. R. Dowling, ''Phase conjugation in underwater acoustics,'' J. Acoust. Soc. Am. **89**, 171–181 (1991).
[12] D. R. Dowling and D. R. Jackson, ''Narrow-band performance of phase-conjugate arrays in dynamic random media,'' J. Acoust. Soc. Am. **91**, 3257–3277 (1992).
[13] F. B. Jensen, W. A. Kuperman, M. B. Porter, and H. Schmidt, *Computational Ocean Acoustics* (AIP Press, Woodbury, NY, 1994).
[14] H. Schmidt and W. A. Kuperman, ''Estimation of surface noise source level from low frequency seismoacoustic ambient noise measurements,'' J. Acoust. Soc. Am. **84**, 2153–2162 (1988).
[15] R. L. Weaver and O. I. Lobkis, ''Elastic wave thermal fluctuations, ultrasonic waveforms by correlation of thermal phonons,'' J. Acoust. Soc. Am. **113**, 2611–2621 (2003).